Robotica (2018) volume 36, pp. 313–332. © Cambridge University Press 2017
doi:10.1017/S0263574717000224

Experimental parameter identification of flexible joint robot manipulators

Roger Miranda-Colorado† and
Javier Moreno-Valenzuela‡*

†*CONACyT-Instituto Politécnico Nacional-CITEDI, Av. Instituto Politécnico Nacional No. 1310, Nueva Tijuana, Tijuana, Baja California, 22435, México. email: rmirandaco@gmail.com*
‡*Instituto Politécnico Nacional-CITEDI, Av. Instituto Politécnico Nacional No. 1310, Nueva Tijuana, Tijuana, Baja California, 22435, México*

(Accepted April 1, 2017. First published online: May 29, 2017)

SUMMARY
This paper contributes by presenting a parameter identification procedure for n-degrees-of-freedom flexible joint robot manipulators. An advantage of the given procedure is the obtaining of robot parameters in a single experiment. Guidelines are provided for the computing of the joint position filtering and velocity estimation. The method relies in the filtered robot model, for which no acceleration measurements are required. The filtered model is expressed in regressor form, which allows applying a parameter identification procedure based on the least squares algorithm. In order to assess the performance of the proposed parameter identification scheme, an implementation of a least squares with forgetting factor (LSFF) parameter identification method is carried out. In order to assess the reliability of the tested identification schemes, a model-based trajectory tracking controller has been implemented twice in different conditions: one control experiment using the estimated parameters provided by the proposed scheme, and another experiment using the parameters given by the LSFF method. These real-time control experiments are compared with respect to numerical simulations using the estimated parameters for each identification method. For the proposed scheme, the comparison between experiments and numerical simulations indicates better accuracy in the torque and position prediction.

KEYWORDS: Flexible joint robot; Least squares; Parameter identification; Robot control; Real-time experiments.

1. Introduction

Much attention has been devoted to applications of robotics in fields, such as service, health care, space robotics, and others. Most applications in these fields require light robot arms able to perform compliant manipulation in contact with a human environment, offering the possibility of energy storage, lower reflected inertia, and higher force control accuracy, with less unintentional damage to the medium.[1] These performance requirements are obtained by increasing the joint flexibility in comparison with that of conventional rigid industrial robots.[2]

Advanced motion controller design requires a complete and accurate dynamic model of robot manipulators.[3] The methodologies for controlling flexible joint robot (FJR) manipulators may include state feedback controllers,[4–7] passivity-based impedance control,[8,9] adaptive techniques,[10–15] sliding mode control,[16] fuzzy logic control,[17] higher-order differential feedback control,[18] among others. In particular, model-based control strategies for robot manipulators have confirmed their potential and reliability even for industrial setups.[19,20] However, model-based control architectures rely on knowing the system parameters. The need thus emerges of resorting to methods of parameter identification.

* Corresponding author. E-mail: moreno@citedi.mx

As in ref. [21], the experimental robot identification procedure proposed in this paper follows these steps:

- modelling,
- experimental design,
- data acquisition,
- signal processing,
- parameter estimation, and
- model validation.

Parameter identification techniques can be categorized as *off-line* and *on-line* methods.[23] The off-line methods are based on collecting all the input–output data, performing data pre-processing, and implementing the identification algorithm. The on-line identification techniques update the estimated parameters in real-time using the on-line measured data during robot operation. In both cases, the robot input–output signals are recorded while the robot is tracking the desired trajectories, which is usually done through the implementation of a robust closed-loop controller. Then, an over determined linear system is created and solved using numerical optimization methods such as the least squares (LS) method,[22] Kalman filtering or the maximum-likelihood method.[23]

This paper is focused in the category of off-line techniques, using the LS algorithm, and is also devoted to provide specific guidelines for accurate parameter identification methodology of FJR manipulators.

In the literature, a large amount of papers have dealt with parameter identification. However, to the best of the authors' knowledge, complete and satisfactory results about the model of FJR are not available. For instance in ref. [2], the parameters of a seven degrees of freedom (DOF) FJR were split into groups, and then independent identification experiments for each group are implemented. In ref. [22], the inertia parameters of the Staubli RX-60 robot were identified using a particle swarm optimization technique and the LS method. Joint stiffness of a FJR was identified in ref. [25] using the LS algorithm, including conditions for a good data processing before identification. Motion capture was used in ref. [26] for dynamic parameter identification of a FJR, in which the identification process is separated into two steps. In ref. [27], the parameters corresponding to the hysteresis and backlash were identified for a FJR. The parameters corresponding to the actuator, drive train, and load of a humanoid robot were estimated in ref. [28]. There, the authors did not obtain precise results due to a deficient estimation of the friction model. Finally, more complex identification procedures for parameter identification of FJR manipulators were given in refs. [29] and [30]. Specifically, in the work,[29] the elements of the gravity vector and the inertia matrix for the KUKA LWR were identified. However, some simplifications were done, which may introduce errors in the estimations. The work in ref. [30] reported a regressor-based methodology that allows estimating all the dynamic parameters, but only simulations results were provided.

The previous literature review reveals that the results on parameter identification of FJR were focused on the identification of a subset of parameters, divided the identification process using different identification experiments, or did not provide experimental results. Then, a study presenting an efficient parameter identification procedure, describing all the steps required to successfully identify the parameters of a FJR manipulator, is absent. Hence, this paper aims to fill this gap by

- providing a complete systematic procedure for parameter identification of FJR manipulators, in which all the system parameters are identified off-line in a single experiment;
- presenting experimental results in a 2-DOF FJR manipulator; and
- validating the results of the parameter identification methodology through real-time experiments.

In the novel parameter identification methodology, the robot parameters are estimated using a filtered regressor form, in which only input torque, motor position, and link position measurements are needed. In order to collect data, a robust controller is implemented. This controller relies in an on-line estimation of motor and link velocities. For the identification algorithm, motor and link velocities are computed off-line by a central differentiation algorithm. Guidelines indicating how to perform these estimations are also given.

In order to assess the performance of the proposed identification procedure, LSFF identification method has been implemented under the same conditions considered for the proposed parameter identification scheme.

https://doi.org/10.1017/S0263574717000224 Published online by Cambridge University Press

The estimated parameters are validated by using a direct validation (DV) method. Besides, a torque and position prediction approach is presented. In both cases, the experimental results are compared to a numerical simulation using the estimated parameters. The validation stage also includes the design of a model-based tracking controller studied in ref. [32]. The methodology to implement the controller used in the validations is also provided in this paper. It is noteworthy to say that the validation tests have also been performed for the estimated parameters obtained by the LSFF method. Better results are obtained with the proposed identification procedure.

From the results obtained in the validation stage, it is concluded that the proposed methodology allows estimating the dynamic parameters of an n-DOF FJR manipulator accurately in a single experiment. Furthermore, the mathematical model obtained with the proposed parameter identification procedure allows predicting the actuator torque and position of the robot manipulator with smaller errors.

The paper is organized as follows. Section 2 presents the mathematical description of the FJR manipulator and the proposed parameter identification procedure. Here, the construction of the regressor, the procedure that allows identifying the system parameters with the filtered robot model (without requiring acceleration measurements), the off-line velocity estimation, and the data pre-processing algorithm are detailed. The experimental results for a Quanser 2-DOF FJR manipulator are given in Section 3. The validation of the estimated parameters for the proposed identification scheme and the LSFF method is analyzed in Section 4 by using DV and the torque and position prediction accuracy approach. Finally, Section 5 contains some concluding remarks.

2. Parameter Identification Procedure

This Section presents the proposed procedure used to identify the parameters of a n-DOF FJR manipulator. In the following, under the modelling assumptions given in ref. [33], the mathematical description of the FJR manipulator is obtained.

2.1. Description of the FJR manipulator

Consider a n-DOF FJR manipulator with revolute joints actuated by direct current (DC) motors. The elasticity of the i-th joint is modelled as a linear torsional spring with stiffness k_{si}, $i = 1, \ldots, n$, which implies that the rotor of each actuator can be modelled as an additional rigid body in the chain with its own inertia. Furthermore, it is assumed that the elastic forces are limited to the linear range of operation.

Figure 1 shows a schematic representation of a n-DOF elastic joint robot manipulator. In this figure, each rotor is coupled to the link by means of a torsional spring. Variable q_i, $i = 1, \ldots, n$ corresponds to the position of link i, which is measured around the z_i axis, according to the Denavit–Hartenberg convention.[34,35] The variable ϕ_i, $i = 1, \ldots, n$, stands for the position of rotor i after the gear box. A counter-clockwise displacement of the rotors or the links corresponds to a positive angular displacement of the rotor or the link, respectively.

Using the Euler–Lagrange equations of motion,[35–37] the dynamic equations of a n-DOF FJR manipulator can be written as follows:

$$\begin{aligned} M_1(\boldsymbol{q})\ddot{\boldsymbol{q}} + C_A(\boldsymbol{q}, \dot{\boldsymbol{q}})\dot{\boldsymbol{q}} + \boldsymbol{f}_1(\dot{\boldsymbol{q}}) + \boldsymbol{g}(\boldsymbol{q}) + K[\boldsymbol{q} - \boldsymbol{\phi}] = 0, \\ M_2\ddot{\boldsymbol{\phi}} + \boldsymbol{f}_2(\dot{\boldsymbol{\phi}}) + K[\boldsymbol{\phi} - \boldsymbol{q}] = \boldsymbol{\tau}, \end{aligned} \tag{1}$$

with

$$\begin{aligned} \boldsymbol{q} &= [\, q_1 \quad \ldots \quad q_n \,]^T \in \mathbb{R}^n, \\ \boldsymbol{\phi} &= [\, \phi_1 \quad \ldots \quad \phi_n \,]^T \in \mathbb{R}^n, \\ \boldsymbol{f}_1(\dot{\boldsymbol{q}}) &= F_{v1}\dot{\boldsymbol{q}} + \boldsymbol{f}_{c1}(\dot{\boldsymbol{q}}), \\ \boldsymbol{f}_2(\dot{\boldsymbol{\phi}}) &= F_{v2}\dot{\boldsymbol{\phi}} + \boldsymbol{f}_{c2}(\dot{\boldsymbol{\phi}}), \end{aligned}$$

https://doi.org/10.1017/S0263574717000224 Published online by Cambridge University Press

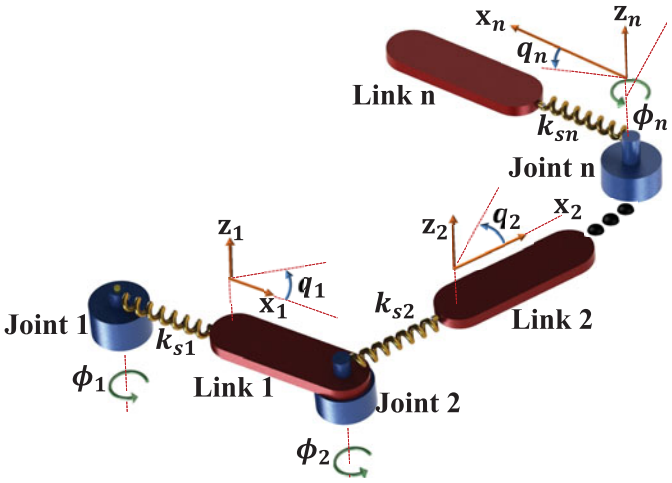

Fig. 1. Representation of a n-DOF flexible joint robot manipulator.

$$\begin{aligned}
\boldsymbol{f}_{c1}(\dot{\boldsymbol{q}}) &= \left[\, f_{c1,1}\tanh(\beta\dot{q}_1) \quad \ldots \quad f_{c1,n}\tanh(\beta\dot{q}_n) \,\right]^T \in \mathbb{R}^n, \\
\boldsymbol{f}_{c2}(\dot{\boldsymbol{\phi}}) &= \left[\, f_{c2,1}\tanh(\beta\dot{\phi}_1) \quad \ldots \quad f_{c2,n}\tanh(\beta\dot{\phi}_n) \,\right]^T \in \mathbb{R}^n, \\
\boldsymbol{\tau} &= \left[\, \tau_1 \quad \ldots \quad \tau_n \,\right]^T \in \mathbb{R}^n,
\end{aligned} \tag{2}$$

where $M_1(\boldsymbol{q}) \in \mathbb{R}^{n\times n}$ is the mass matrix depending only of link displacements, M_2 is the matrix containing the rotor inertias, $C_A(\boldsymbol{q}, \dot{\boldsymbol{q}})\dot{\boldsymbol{q}} \in \mathbb{R}^n$ is the vector of centrifugal and Coriolis forces, $\boldsymbol{g}(\boldsymbol{q}) \in \mathbb{R}^n$ is the vector of gravitational torques or forces, $K \in \mathbb{R}^{n\times n}$ is the matrix associated with the spring stiffness, $F_{vi} \in \mathbb{R}^{n\times n}$, $i = 1, 2$, are the matrices containing the viscous friction coefficients. The vectors $\boldsymbol{f}_{c1}(\dot{\boldsymbol{q}})$, $\boldsymbol{f}_{c2}(\dot{\boldsymbol{\phi}}) \in \mathbb{R}^n$ correspond to the continuous version of the Coulomb friction with $\beta > 0$ large enough; $\boldsymbol{\tau} \in \mathbb{R}^n$ is the torque input vector; $\boldsymbol{q}, \boldsymbol{\phi}$ are the link and rotor position vectors, and $\dot{\boldsymbol{q}}, \dot{\boldsymbol{\phi}}$ are the link and rotor velocity vectors, respectively.

We assume that the DC motors delivering torque at the joints are driven by servo amplifiers configured in current mode.[38] Hence, the torques applied at the joints are related with the motor current as

$$\boldsymbol{\tau}(t) = K_m \boldsymbol{i}_m(t), \tag{3}$$

where $\boldsymbol{i}_m \in \mathbb{R}^n$ is the motor current vector, and $K_m \in \mathbb{R}^{n\times n}$ is a diagonal matrix containing the motor torque constants. Considering this servo amplifier configuration, the actual motor current becomes

$$\boldsymbol{i}_m(t) = \boldsymbol{i}_d(t) = K_{sa}\boldsymbol{u}(t), \tag{4}$$

with $\boldsymbol{i}_d(t) \in \mathbb{R}^n$ being the desired motor current vector, $K_{sa} \in \mathbb{R}^{n\times n}$ a diagonal matrix with the servo amplifier gains, and $\boldsymbol{u}(t) \in \mathbb{R}^n$ the servo amplifier input voltage. Therefore, from Eqs. (3) to (4), the DC motor output torques are given by

$$\boldsymbol{\tau}(t) = K_m K_{sa}\boldsymbol{u}(t), \tag{5}$$

indicating that the delivered torque is proportional to the input servo amplifier voltage.

In this paper, the applied torque $\boldsymbol{\tau}(t)$ is considered to be measured by using the relationship Eq. (5), under the assumption that matrices K_m and K_{sa} are known.

https://doi.org/10.1017/S0263574717000224 Published online by Cambridge University Press

2.2. Filtered dynamic model

Model identification methods for rigid robot manipulators rely on the linear parameterization property of the robot dynamic equations.[39,40] As a matter of fact, a similar factorization holds also for FJR manipulators, presenting two cases:[41] when only link positions $\boldsymbol{q}$ are available, and when both the motor position $\boldsymbol{\phi}$ and link position $\boldsymbol{q}$ can be measured. We consider the latter case study, whereby Eq. (1) can be rewritten as

$$Y(\boldsymbol{x}, \dot{\boldsymbol{x}}, \ddot{\boldsymbol{x}})\boldsymbol{\theta} = \boldsymbol{\vartheta}, \tag{6}$$

where $\boldsymbol{x} = [\boldsymbol{q}^T, \boldsymbol{\phi}^T]^T \in \mathbb{R}^{2n}$ is the composed configuration vector, $Y(\boldsymbol{x}, \dot{\boldsymbol{x}}, \ddot{\boldsymbol{x}}) \in \mathbb{R}^{2n \times p}$ is the regression matrix, $\boldsymbol{\theta} \in \mathbb{R}^p$ is the parameter vector, and

$$\boldsymbol{\vartheta} = \begin{bmatrix} \mathbf{0}_{n\times 1} \\ \boldsymbol{\tau} \end{bmatrix} \in \mathbb{R}^{2n} \tag{7}$$

is the input of the regressor system Eq. (6), being $\mathbf{0}_{n\times 1}$ a null column vector in $\mathbb{R}^n$.

Acceleration measurements in computing $Y(\boldsymbol{x}, \dot{\boldsymbol{x}}, \ddot{\boldsymbol{x}})$ are avoided by computing a filtered version of the model (6). See for example ref. [42–44], where filtered models were used for parameter identification of rigid link manipulators. With this aim, note that (6) can be rewritten as the first order differential equation

$$\left[\frac{d}{dt} Y_a(\boldsymbol{x}, \dot{\boldsymbol{x}}) + Y_b(\boldsymbol{x}, \dot{\boldsymbol{x}})\right]\boldsymbol{\theta} = \boldsymbol{\vartheta}, \tag{8}$$

where

$$\begin{aligned}
Y_a(\boldsymbol{x}, \dot{\boldsymbol{x}})\boldsymbol{\theta} &= M(\boldsymbol{x})\dot{\boldsymbol{x}}, \\
Y_b(\boldsymbol{x}, \dot{\boldsymbol{x}})\boldsymbol{\theta} &= -\dot{M}(\boldsymbol{x})\dot{\boldsymbol{x}} + C(\boldsymbol{x}, \dot{\boldsymbol{x}})\dot{\boldsymbol{x}} + F_v\dot{\boldsymbol{x}} + \boldsymbol{f}_c(\dot{\boldsymbol{x}}) + G(\boldsymbol{x}) + K_e\boldsymbol{x}, \\
M(\boldsymbol{x}) &= \begin{bmatrix} M_1(\boldsymbol{q}) & \mathbf{0}_{n\times n} \\ \mathbf{0}_{n\times n} & M_2 \end{bmatrix}, \; C(\boldsymbol{x}, \dot{\boldsymbol{x}}) = \begin{bmatrix} C_A(\boldsymbol{q}, \dot{\boldsymbol{q}}) & \mathbf{0}_{n\times n} \\ \mathbf{0}_{n\times n} & \mathbf{0}_{n\times n} \end{bmatrix}, \; G(\boldsymbol{x}) = \begin{bmatrix} \boldsymbol{g}(\boldsymbol{q}) \\ \mathbf{0}_{n\times 1} \end{bmatrix} \\
F_v &= \begin{bmatrix} F_{v1} & \mathbf{0}_{n\times n} \\ \mathbf{0}_{n\times n} & F_{v2} \end{bmatrix}, \; \boldsymbol{f}_c(\dot{\boldsymbol{x}}) = \begin{bmatrix} \boldsymbol{f}_{c1}(\dot{\boldsymbol{q}}) \\ \boldsymbol{f}_{c2}(\dot{\boldsymbol{\phi}}) \end{bmatrix}, \; K_e = \begin{bmatrix} K & -K \\ -K & K \end{bmatrix},
\end{aligned}$$

and $\mathbf{0}_{n\times n}$ is the null matrix in $\mathbb{R}^{n\times n}$.

Similarly to ref. [42], in order to obtain a filtered model of Eq. (1), we use the following low-pass filter:

$$f(s) = \frac{\lambda}{s + \lambda}, \tag{9}$$

with $\lambda \in \mathbb{R}^+$ denoting the cut-off frequency, and s being the Laplace variable.

By multiplying Eq. (8) by $f(s)$, we obtain the so-called *filtered dynamic model*

$$Y_f(\boldsymbol{x}, \dot{\boldsymbol{x}})\boldsymbol{\theta} = \boldsymbol{\vartheta}_f, \tag{10}$$

where

$$\begin{aligned}
\boldsymbol{\vartheta}_f &= f(s)\boldsymbol{\vartheta}, \\
Y_f(\boldsymbol{x}, \dot{\boldsymbol{x}}) &= Y_{af}(\boldsymbol{x}, \dot{\boldsymbol{x}}) + Y_{bf}(\boldsymbol{x}, \dot{\boldsymbol{x}}), \\
Y_{af}(\boldsymbol{x}, \dot{\boldsymbol{x}}) &= sf(s)Y_a(\boldsymbol{x}, \dot{\boldsymbol{x}}), \\
Y_{bf}(\boldsymbol{x}, \dot{\boldsymbol{x}}) &= f(s)Y_b(\boldsymbol{x}, \dot{\boldsymbol{x}}).
\end{aligned} \tag{11}$$

https://doi.org/10.1017/S0263574717000224 Published online by Cambridge University Press

In form of integral equation and assuming null initial conditions, the filtered signals given in Eq. (11) can be expressed as

$$\begin{aligned} \boldsymbol{\vartheta}_f(t) &= \lambda\left[\int_0^t [\boldsymbol{\vartheta}(\sigma) - \boldsymbol{\vartheta}_f(\sigma)]d\sigma\right], \\ Y_{af}(t) &= \lambda\left[Y_a(t) - \int_0^t Y_{af}(\sigma)d\sigma\right], \\ Y_{bf}(t) &= \lambda\int_0^t \left[Y_b(\sigma) - Y_{bf}(\sigma)\right]d\sigma. \end{aligned} \tag{12}$$

In practice, discrete robot motion measurements are available. Then, the filtered dynamic model (10) can be implemented by discretizing the filter $f(s)$ in Eq. (9) and

$$g(s) = sf(s), \tag{13}$$

using the zero-order hold[45]

$$G_0(s) = \frac{(1 - e^{-sT})}{s}, \tag{14}$$

and the relations[45]

$$\mathcal{Z}\left\{e^{-kTs}\right\} = z^{-k}, \tag{15}$$

$$\mathcal{Z}\left\{\frac{1}{s}\right\} = \frac{z}{z-1}, \tag{16}$$

$$\mathcal{Z}\left\{\frac{1}{s+a}\right\} = \frac{z}{z - e^{-aT}}, \tag{17}$$

where $\mathcal{Z}\{\cdot\}$ is the z-trasform operator, $k = 0, 1, \ldots$ is the integer time index, and $T[s]$ is the sampling period.

By substituting Eq. (14) into Eqs. (9) and (13) yields

$$\begin{aligned} \bar{f}(s) = G_0(s)f(s) &= [1 - e^{-Ts}]\left[\frac{\lambda}{s(s+\lambda)}\right], \\ \bar{g}(s) = G_0(s)g(s) &= [1 - e^{-Ts}]\left[\frac{\lambda}{s+\lambda}\right], \end{aligned} \tag{18}$$

and, by using Eqs. (15)–(17), we obtain

$$f_D(z) = \frac{1 - e^{-\lambda T}}{z - e^{-\lambda T}}, \tag{19}$$

$$g_D(z) = \frac{\lambda z - \lambda}{z - e^{-\lambda T}}, \tag{20}$$

where $f_D(z)$ in Eq. (19) and $g_D(z)$ in Eq. (20) are the discrete representation of $f(s)$ in Eq. (9) and $g(s)$ in Eq. (13), respectively.

The discrete version of $Y_{af}(t)$ and $Y_{bf}(t)$ are then given by

$$Y_{af}(kT) = g_D(z)Y_a(kT), \tag{21}$$

and

$$Y_{bf}(kT) = f_D(z)Y_b(kT), \tag{22}$$

https://doi.org/10.1017/S0263574717000224 Published online by Cambridge University Press

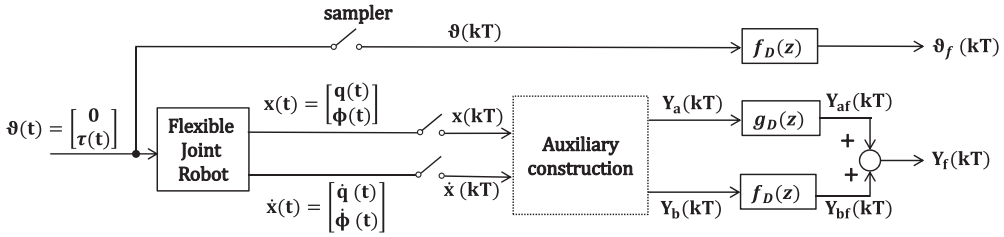

Fig. 2. Block diagram representation of the derivation of the discrete filtered model (23). The block 'auxiliary construction'means the operations to build matrices $Y_a(kT)$ and $Y_b(kT)$.

In this work, the filtered model (10) was implemented using Eqs. (19) and (20) with the Matlab function `filter(A,B,D)`, where `A,B` are the coefficients of the numerator and denominator, and `D` corresponds to the signal to be filtered.

2.3. Identification procedure

Now, we assume that only discrete measurements of the position $\boldsymbol{x}(kT)$ and velocity $\dot{\boldsymbol{x}}(kT)$ are available. Then, let us consider the next discrete filtered model of the FJR manipulator

$$Y_f(kT)\boldsymbol{\theta} = \boldsymbol{\vartheta}_f(kT), \tag{23}$$

where

$$Y_f(kT) = g_D(z)Y_a(kT) + f_D(z)Y_b(kT),$$
$$\boldsymbol{\vartheta}_f(kT) = f_D(z)\boldsymbol{\vartheta}(kT).$$

Figure 2 represents the way the discrete filtered model (23) is derived. The block 'auxiliary construction' includes the operations required to build the matrices $Y_a(kT)$ and $Y_b(kT)$.

In practice, different types of disturbances, such as quantization noise of the encoder, pulse width modulation (PWM) switching noise of the servo amplifiers, and errors due to velocity estimation, affect the robot. Therefore, special attention is paid to the off-line filtering of the position and computation of the velocity.

The proposed identification method is performed off-line by using time series of the measured input $\boldsymbol{\tau}(kT)$, required in the generalized input $\boldsymbol{\vartheta}(kT)$ in (7), and the measured positions $\boldsymbol{q}(kT)$ and $\boldsymbol{\phi}(kT)$, which are components of the generalized configuration vector $\boldsymbol{x}(kT)$.

2.3.1. Controller selection. A good set of estimated parameters is obtained if an appropriate identification experiment is performed. This experimental stage involves the design of a reference trajectory exciting all the system dynamics. In this work, the robot dynamics is excited using the next PD controller

$$\boldsymbol{\tau} = K_p\tilde{\boldsymbol{\phi}} + K_v\dot{\tilde{\boldsymbol{\phi}}}, \tag{24}$$

where K_p, $K_v \in \mathbb{R}^{n\times n}$ are diagonal matrices. The vector $\tilde{\boldsymbol{\phi}} = \boldsymbol{\phi}_d - \boldsymbol{\phi}$ denotes the rotor position error, $\dot{\tilde{\boldsymbol{\phi}}} = \dot{\boldsymbol{\phi}}_d - \dot{\boldsymbol{\phi}}$ is the rotor velocity error, and $\boldsymbol{\phi}_d(t) \in \mathbb{R}^n$ is the rotor reference trajectory.

Note that a PD controller provides a relative low tracking error, which is important for the excitation of the robot dynamics in the parameter identification process. See for example ref. [46], where a PD controller was used to generate time series of inputs and outputs for robot parameter identification.

2.3.2. On-line velocity estimation. To implement on-line the PD controller Eq. (24), a velocity estimator is used. First, consider the polynomials given in terms of the z-transform

$$Q_1(z^{-1}) = 1 + z^{-1} + z^{-2} + \cdots + z^{-p_1},$$
$$Q_2(z^{-1}) = 1 + z^{-1} + z^{-2} + \cdots + z^{-p_2},$$

https://doi.org/10.1017/S0263574717000224 Published online by Cambridge University Press

where p_1, $p_2 \in \mathbb{N}$. The averaged position $\bar{\boldsymbol{\phi}}(kT)$ of the last $p_1 + 1$ samples is given by

$$\bar{\boldsymbol{\phi}}(kT) = \frac{Q_1(z^{-1})}{p_1 + 1}\boldsymbol{\phi}(kT), \tag{25}$$

where k is the integer time index, $T[s]$ is the sampling period, and the product kT is the discrete time. Thus, the dirty derivative of $\bar{\boldsymbol{\phi}}(kT)$ is given by

$$\dot{\bar{\boldsymbol{\phi}}}(kT) = \frac{1 - z^{-1}}{T}\bar{\boldsymbol{\phi}}(kT).$$

Finally, the rotor velocity can be approached by averaging the last $p_2 + 1$ samples of $\dot{\bar{\boldsymbol{\phi}}}(kT)$, i.e.,

$$\dot{\boldsymbol{\phi}}(kT) \approx \frac{Q_2(z^{-1})}{p_2 + 1}\dot{\bar{\boldsymbol{\phi}}}(kT). \tag{26}$$

2.3.3. Quantization error. As indicated above, disturbances may affect the performance of the identification process. In order to reduce such effects, some data pre-processing can be performed. Note that the elements of the regression matrix $Y_f(kT)$ in Eq. (23) depend on $\boldsymbol{x}(kT), \dot{\boldsymbol{x}}(kT)$. However, in most cases industrial robots are only equipped with optical encoders as position sensors, which introduce quantization error. Furthermore, if $Y_f(kT)$ and $\boldsymbol{\vartheta}_f(kT)$ are obtained from noisy measurements, the parameter estimates may be far away from their actual values.

Quantization error can be reduced by filtering position measurements through a low-pass non-causal zero-phase digital filter with cut-off frequency ω_{fq}. This is accomplished in Matlab by using a low-pass Butterworth filter in both the forward and reverse direction using the *filtfilt* function. This filter has a flat amplitude characteristic without phase shift in the range $[0, \omega_{fq}]$ and zero phase distortion.

2.3.4. Off-line velocity estimation. Computation of the filtered regressor matrix $Y_f(\boldsymbol{x}, \dot{\boldsymbol{x}})$ requires velocity values. Velocity sensors are not usually available in manipulators. Furthermore, joint velocity obtained by numerical differentiation amplifies the quantization error because differentiation behaves as a high-pass filter. Then, to compute $Y_f(\boldsymbol{x}, \dot{\boldsymbol{x}})$ we have to resort to a procedure for off-line velocity estimation as a previous step.

A velocity estimation procedure requires a good signal-to-noise ratio and a group delay as small as possible. In this work, the estimated velocity required for computing $Y_f(kT)$ were obtained by using the central differentiation algorithm

$$\dot{\boldsymbol{x}}(kT) = \frac{\boldsymbol{x}_f([k+1]T) - \boldsymbol{x}_f([k-1]T)}{2T}, \tag{27}$$

where k is the integer time index, $T[s]$ is the sampling period, and $\boldsymbol{x}_f(kT) \in \mathbb{R}^{2n}$ is the filtered generalized position vector, obtained after using the *filtfilt* function.

Using the aforementioned data pre-processing, the proposed parameter identification algorithm can be applied to the model (23).

2.3.5. LS parameter estimation. The estimated values of the parameter vector $\boldsymbol{\theta} \in \mathbb{R}^p$ can be obtained using the LS algorithm given by ref. [47]

$$\hat{\boldsymbol{\theta}}(kT) = \left[\sum_{i=0}^{k} Y_f^T(iT)Y_f(iT)\right]^{-1} \sum_{i=0}^{k} Y_f^T(iT)\boldsymbol{\vartheta}_f(iT), \tag{28}$$

where $\hat{\boldsymbol{\theta}}(kT) \in \mathbb{R}^p$ is the estimate of $\boldsymbol{\theta}$ at the discrete time instant kT, with $0 \leq k \leq N - 1$, and N is the number of samples.

The parameters of a n-DOF FJR manipulator described by Eq. (1) can be identified by following all the steps described above.

https://doi.org/10.1017/S0263574717000224 Published online by Cambridge University Press

Table I. DH parameters of the 2-DOF FJR manipulator.

Link	α_{i-1}	a_{i-1}	d_i	θ_i
1	0	0	0	q_1
2	0	L_1	0	q_2

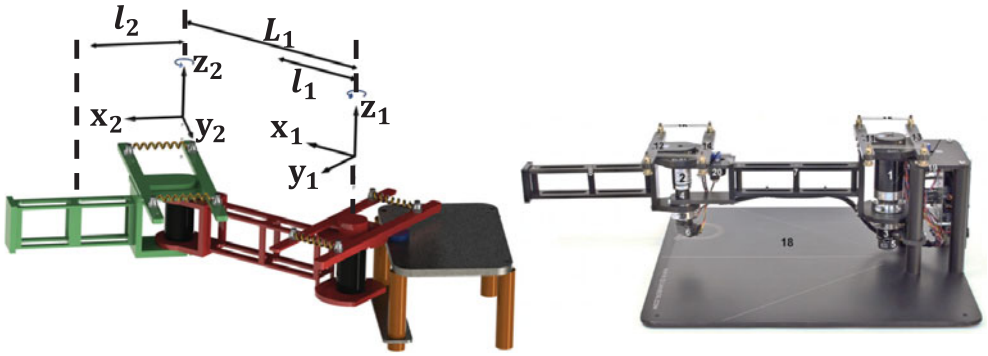

Fig. 3. Two representations of the flexible joint robot manipulator. (a) Approximated computed-aided design, and (b) picture of the actual system at its home position.

It is important to remark that the initial error in tracking the desired reference for the parameter identification experiments acts as a disturbance to the estimation error. However, this does not affect the properties of the parameter estimation algorithm, but only affects the transient response of the estimated parameters.[48]

In the next, an experimental verification of the parameter identification procedure is given.

3. Experimental Parameter Identification

The parameter identification procedure described in Section 2 is now applied to the Quanser 2-DOF FJR manipulator[31] depicted in Fig. 3. In this robot, the joints exhibit visible harmonics during accelerations, while the links are rigid in comparison. The system has two DC motors, the Maxon 273759 and 118752 for joints 1 and 2, respectively. Each motor drives harmonic gearboxes with null backlash in a two-bar serial linkage. Both links are rigid, the primary is coupled to the first drive by means of a flexible joint, and it carries at its end the second harmonic drive, which is coupled to the second rigid link via another flexible joint. The data are obtained using the data acquisition device (DAQ) Q8-USB, which has analogue and digital inputs/outputs, encoder inputs, and PWM outputs. This device is optimized for real-time control and allows interacting with Matlab/Simulink using the Quanser QUARC and RPC toolkit control software. Real-time experiments are performed through Real-Time Windows Target libraries. Both motors and flexible joints are instrumented with quadrature optical encoders of 4096 pulses per revolution (ppr).

The motors are powered using the power amplifier Quanser AMPAQ current amplifier. The power amplifier is equipped with current sensors, so that the actual current values are measured using the DAQ Q8-USB. Then, by using Eq. (3), it is possible to obtain the values corresponding to the torque vector $\boldsymbol{\tau}(t)$. Measurements corresponding to the link position $\boldsymbol{q}(t)$ and the joint position $\boldsymbol{\phi}(t)$ are obtained using the system optical encoders.

Figure 3(a) shows a computer-aided model of the robot manipulator, together with the reference frames chosen according to Denavit–Hartenberg convention.[34,35] The associated Denavit–Hartenberg parameters are given in Table I. In this model, each rotor is coupled to the link by means of a torsional

https://doi.org/10.1017/S0263574717000224 Published online by Cambridge University Press

Table II. Parameters θ_i, $i = 1, \ldots, 15$ for the 2-DOF flexible joint robot.

Parameter	Definition	Parameter	Definition
θ_1	$(m_{l1} + m_{r1})l_1^2 + I_{lzz1} + I_{lzz2}$	θ_9	f_{v4}
	$+(m_{l2} + m_{r2})(L_1^2 + l_2^2)$	θ_{10}	k_{s1}
θ_2	$(m_{l2} + m_{r2})L_1 l_2$	θ_{11}	k_{s2}
θ_3	$(m_{l2} + m_{r2})l_2^2 + I_{lzz2}$	θ_{12}	f_{c1}
θ_4	$r_1^2 I_{rzz1}$	θ_{13}	f_{c2}
θ_5	$r_2^2 I_{rzz2}$	θ_{14}	f_{c3}
θ_6	f_{v1}	θ_{15}	f_{c4}
θ_7	f_{v2}		
θ_8	f_{v3}		

spring. Figure 3(b) depicts the actual robot used in the identification experiments at its home position. Note that the FJR manipulator to be identified is a planar robot moving in the horizontal plane, thus being not affected by gravity.

Using the Euler–Lagrange equations of motion,[36,37] the robot dynamic equations can be expressed in the form Eq.(1) with:

$$
\begin{aligned}
\boldsymbol{q} &= [\, q_1 \quad q_2 \,]^T \in \mathbb{R}^2,\ \boldsymbol{\phi} = [\, \phi_1 \quad \phi_2 \,]^T \in \mathbb{R}^2, \\
\boldsymbol{\tau} &= \begin{bmatrix} \tau_1 & \tau_2 \end{bmatrix}^T,\ \boldsymbol{\theta} = \begin{bmatrix} \theta_1 & \ldots & \theta_{15} \end{bmatrix}^T, \\
M_1(\boldsymbol{q}) &= \begin{bmatrix} \theta_1 + 2\theta_2 \cos(q_2) & \theta_2 \cos(q_2) + \theta_3 \\ \theta_2 \cos(q_2) + \theta_3 & \theta_3 \end{bmatrix},\ M_2 = \begin{bmatrix} \theta_4 & 0 \\ 0 & \theta_5 \end{bmatrix}, \\
C_A(\boldsymbol{q}, \dot{\boldsymbol{q}}) &= \begin{bmatrix} -\theta_2 \dot{q}_2 \sin(q_2) & -\theta_2(\dot{q}_1 + \dot{q}_2)\sin(q_2) \\ \theta_2 \dot{q}_1 \sin(q_2) & 0 \end{bmatrix}, \\
F_{v1} &= \begin{bmatrix} \theta_6 & 0 \\ 0 & \theta_7 \end{bmatrix},\ F_{v2} = \begin{bmatrix} \theta_8 & 0 \\ 0 & \theta_9 \end{bmatrix},\ K = \begin{bmatrix} \theta_{10} & 0 \\ 0 & \theta_{11} \end{bmatrix}, \\
\boldsymbol{f}_{c1}(\dot{\boldsymbol{q}}) &= \begin{bmatrix} \theta_{12} \tanh(\beta \dot{q}_1) \\ \theta_{13} \tanh(\beta \dot{q}_2) \end{bmatrix},\ \boldsymbol{f}_{c2}(\dot{\boldsymbol{\phi}}) = \begin{bmatrix} \theta_{14} \tanh(\beta \dot{\phi}_1) \\ \theta_{15} \tanh(\beta \dot{\phi}_2) \end{bmatrix}.
\end{aligned}
$$

Variables q_1 and q_2 correspond to the position of link 1 and link 2, respectively, while ϕ_1 and ϕ_2 stand for the position of rotor 1 and rotor 2 after the gear box, respectively. Parameters $\boldsymbol{\theta} \in \mathbb{R}^{15}$ are described in Table II using the following notation:

m_{li}	mass of link i, $i = 1, 2$,
m_{ri}	mass of rotor i, $i = 1, 2$,
L_1	length of link 1,
l_i	distance to the centre of gravity of link i, $i = 1, 2$,
I_{lzzi}	principal inertia moment at z axis of link i, $i = 1, 2$,
I_{rzzi}	principal inertia moment at z axis of rotor i, $i = 1, 2$,
r_i	gear ratio of actuator i, $i = 1, 2$,
k_{si}	FJR torsional stiffness of spring i, $i = 1, 2$,
f_{v1}, f_{v2}	viscous friction coefficient of link 1 and 2, respectively,
f_{v3}, f_{v4}	viscous friction coefficient of joint 1 and 2, respectively,
f_{ci}	Coulomb friction coefficient of link i, $i = 1, 2$,
f_{c3}, f_{c4}	Coulomb friction coefficient of joint 1 and 2, respectively.

https://doi.org/10.1017/S0263574717000224 Published online by Cambridge University Press

The corresponding matrices $Y_a(\boldsymbol{x}, \dot{\boldsymbol{x}})$, $Y_b(\boldsymbol{x}, \dot{\boldsymbol{x}}) \in \mathbb{R}^{4\times 15}$ of Eq. (8) have the following definition:

$$Y_a = \left[\, Y_{a1}(\boldsymbol{x}, \dot{\boldsymbol{x}}) \quad \mathbf{0}_{4\times 10} \,\right],$$

$$Y_{a1} = \begin{bmatrix} \dot{q}_1 & 2(\dot{q}_1+\dot{q}_2)\cos(q_2) & \dot{q}_2 & 0 & 0 \\ 0 & \cos(q_2)\dot{q}_1 & \dot{q}_1+\dot{q}_2 & 0 & 0 \\ 0 & 0 & 0 & \dot{\phi}_1 & 0 \\ 0 & 0 & 0 & 0 & \dot{\phi}_2 \end{bmatrix},$$

$$Y_b = \left[\, Y_{b1} \quad Y_{b2} \quad Y_{b3} \quad Y_{b4} \,\right],$$

$$Y_{b1} = \begin{bmatrix} 0 & 0 & 0 & 0 \\ 0 & (\dot{q}_1\dot{q}_2+\dot{q}_1^2)\sin(q_2) & 0 & 0 \\ 0 & 0 & 0 & 0 \\ 0 & 0 & 0 & 0 \end{bmatrix}, \; Y_{b2} = \begin{bmatrix} 0 & \dot{q}_1 & 0 & 0 \\ 0 & 0 & \dot{q}_2 & 0 \\ 0 & 0 & 0 & \dot{\phi}_1 \\ 0 & 0 & 0 & 0 \end{bmatrix},$$

$$Y_{b3} = \begin{bmatrix} 0 & q_1-\phi_1 & 0 \\ 0 & 0 & q_2-\phi_2 \\ 0 & \phi_1-q_1 & 0 \\ \dot{\phi}_2 & 0 & \phi_2-q_2 \end{bmatrix}, \; Y_{b4} = \begin{bmatrix} \mathrm{diag}\{\tanh(\beta q_i)\} & \mathbf{0}_{2\times 2} \\ \mathbf{0}_{2\times 2} & \mathrm{diag}\{\tanh(\beta \phi_i)\} \end{bmatrix},$$

with $i = 1, 2$, and diag$\{\cdot\}$ being a diagonal matrix.

The robot manufacturer provides nominal values of the parameters $\theta_1, \ldots, \theta_{11}$, as indicated in Table III. Furthermore, the motor torque constant matrix K_m and servo amplifier gain matrix K_{sa} are given by

$$K_m = \begin{bmatrix} 0.119 & 0 \\ 0 & 0.0234 \end{bmatrix} [Nm/A], \; K_{sa} = \begin{bmatrix} 0.5 & 0 \\ 0 & 0.5 \end{bmatrix} [A/V],$$

respectively. The desired value of control torque $\boldsymbol{\tau}(t)$ transferred to the mechanism is obtained by inverting the relationship Eq. (5).

The gains of the PD control Eq. (24) were set to

$$K_p = \begin{bmatrix} 50 & 0 \\ 0 & 5 \end{bmatrix} \text{[Nm/rad]}, \; K_v = \begin{bmatrix} 0.05 & 0 \\ 0 & 0.01 \end{bmatrix} \text{[Nm s/rad]},$$

and the velocity values required to implement the PD control were obtained using the velocity approximation Eq. (26) with $p_1 = p_2 = 4$.

For the identification experiments, the reference trajectory

$$\boldsymbol{\phi}_d(t) = 3 \begin{bmatrix} \sin(2\pi t) + \sin(\pi t + \frac{\pi}{6}) + \sin(0.4\pi t + \frac{\pi}{4})) \\ \sin(0.4\pi t) + \sin(2\pi t + \frac{\pi}{5}) + \sin(\pi t + \frac{\pi}{2}) \end{bmatrix} [deg] \tag{29}$$

was used.

Matrix $Y_f(\cdot)$ in Eq. (10) was implemented using the value $\beta = 100$ for the hyperbolic tangent function employed to approach the Coulomb friction vector $\boldsymbol{f}_{c1}(\dot{\boldsymbol{q}})$ at the links, and $\boldsymbol{f}_{c2}(\dot{\boldsymbol{\phi}})$ at the joints. Besides, the filters Eqs. (19)and(20) were implemented using the value $\lambda = 30$, and a sampling period of $T = 1$ [ms].

In order to compare the proposed parameter identification methodology, LSFF algorithm has been implemented on the filtered regression model (23) without any preprocessing. Specifically, by computing in real-time the filtered regression matrix $Y_f(kT)$, and the vector $\boldsymbol{\vartheta}_f(kT)$, we implemented

https://doi.org/10.1017/S0263574717000224 Published online by Cambridge University Press

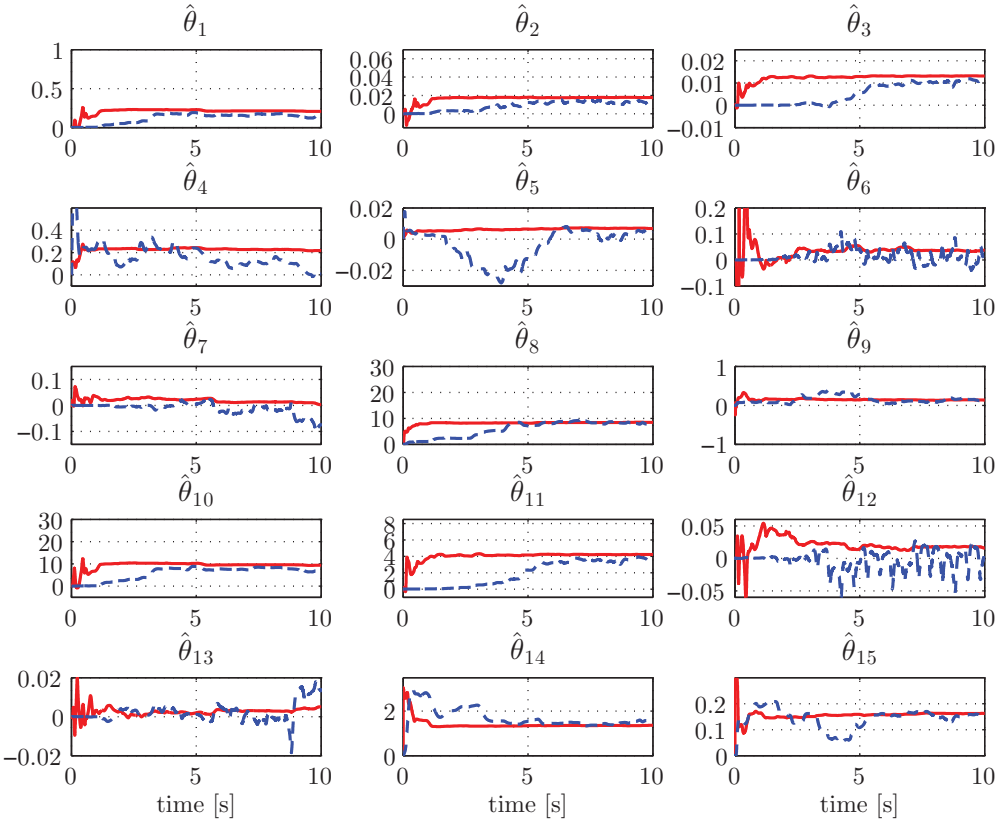

Fig. 4. Estimated parameters $\hat{\boldsymbol{\theta}}(kT)$, $\hat{\boldsymbol{\theta}}_{LSFF}(kT)$ for the 2-DOF FJR manipulator obtained experimentally by using the proposed parameter identification methodology (red line) and the LSFF identification method (dashed blue line).

also in real-time the identification algorithm given by[48]

$$\dot{\hat{\boldsymbol{\theta}}}_{LSFF}(kT) = P(kT)Y_f(kT)\boldsymbol{e}_{LSFF}(kT), \tag{30}$$

$$\boldsymbol{e}_{LSFF}(kT) = \boldsymbol{\vartheta}_f(kT) - \hat{\boldsymbol{\theta}}^T_{LSFF}(kT)Y_f(kT),$$

$$\dot{P}(kT) = \delta P(kT) - P(kT)Y_f(kT)Y_f^T(kT)P(kT),$$

where $\hat{\boldsymbol{\theta}}_{LSFF}$ denotes the estimated value of the parameter vector $\boldsymbol{\theta}$, $\delta \in \mathbb{R}^+$ is the forgetting factor, $P \in \mathbb{R}^{p\times p}$ is a symmetric, positive definite gain matrix, with $P(0) = P^T(0) > 0$, and $\boldsymbol{e}_{LSFF}$ is the LSFF output-error. The values $\delta = 1$ and $P(0) = 10I_{15}$, with I_{15} being the identity matrix in $\mathbb{R}^{15\times 15}$, were used in the parameter identification experiments using the LSFF method in Eq. (30).

For the proposed off-line identification procedure and for the LSFF identification method in Eq. (30), the time evolution of the parameter estimates $\hat{\boldsymbol{\theta}}(kT)$ and $\hat{\boldsymbol{\theta}}_{LSFF}(kT)$ computed for each sample kT is depicted in Fig. 4. Table III shows the nominal values provided by the robot manufacturer, and the corresponding estimated values obtained using Eqs. (28) and (30). These estimated values correspond to those obtained at $10[s]$ after starting the parameter identification experiment. This specific time is large enough for the estimated parameters to reach the steady state. Notice that for the proposed identification algorithm, most of the estimated parameters remain around the same value after $5[s]$. However, for the LSFF identification method, the estimated parameters behave in an oscillatory form, which shows that this identification algorithm is more sensitive to the noise present in the experiment.

It is worth noticing from Table III that the estimated parameters related to the inertias and viscous friction coefficients present a remarkably deviation from the values provided by the manufacturer.

https://doi.org/10.1017/S0263574717000224 Published online by Cambridge University Press

Table III. Nominal and estimated values of the parameters $\theta_i, i = 1, \ldots, 15$ for the 2-DOF FJR using the proposed parameter identification scheme and the LSFF algorithm.

Parameter	Nominal value	Proposed method ($\hat{\boldsymbol{\theta}}$)	LSFF algorithm ($\hat{\boldsymbol{\theta}}_{LSFF}$)
θ_1	0.190807	0.207184	0.140323
θ_2	0.016474	0.017580	0.011038
θ_3	0.010724	0.013163	0.010570
θ_4	0.062800	0.216776	0.008266
θ_5	0.002575	0.006842	0.004597
θ_6	0.070364	0.037675	0.004189
θ_7	0.028211	0.002959	−0.073912
θ_8	4.5	8.435283	8.216284
θ_9	0.5	0.135564	0.090998
θ_{10}	9.0	9.358730	6.929031
θ_{11}	4.0	4.212811	3.638719
θ_{12}	*	0.015771	0.001516
θ_{13}	*	0.005018	0.013101
θ_{14}	*	1.360210	1.523355
θ_{15}	*	0.162529	0.161235

* Not provided by the manufacturer.

In the next Section, a validation study is presented, which has the aim of supporting the accuracy and precision of the proposed identification procedure.

4. Model Validation

A parameter identification process provides an estimated model for an intended application. In order to assess the reliability of the parameter estimates, a validation procedure should be used. The following methods can be used to validate the model:[21,23,24,42]

1. *Direct validation*. Consists in comparing the torque $\boldsymbol{\tau}(t)$ and positions $\boldsymbol{q}(t)$, $\boldsymbol{\phi}(t)$ measured in the identification experiment with respect to the corresponding torque $\hat{\boldsymbol{\tau}}(t)$ and positions $\hat{\boldsymbol{q}}(t)$, $\hat{\boldsymbol{\phi}}(t)$ obtained from a numerical simulation using the estimated parameters.
2. *Torque and position prediction accuracy*. Consists in carrying out a validation experiment with a reference trajectory $\boldsymbol{\phi}_d(t)$ different from the one used in the identification experiment. Then, the actuator torque-prediction accuracy and position-prediction accuracy are compared, i.e., the measured torque $\boldsymbol{\tau}(t)$ and position values $\boldsymbol{q}(t)$, $\boldsymbol{\phi}(t)$ are compared with respect to the numerical torque $\hat{\boldsymbol{\tau}}(t)$ and positions $\hat{\boldsymbol{q}}(t)$, $\hat{\boldsymbol{\phi}}(t)$ obtained from a simulated system using the estimated parameters.

A metric of the prediction accuracy is given by the RMS values, e_{RMS}, of the error signals

$$e_{RMS} = \sqrt{\frac{1}{m}\sum_{i=1}^{m}\epsilon^2(i)}, \tag{31}$$

where $\epsilon(\cdot)$ corresponds to the difference between measured and predicted torque or position, and m is the number of samples.

A block diagram of the DV and the torque and position prediction accuracy validation is given in Fig. 5. The torque $\boldsymbol{\tau}(t)$ and position signals $\boldsymbol{q}(t)$, $\boldsymbol{\phi}(t)$ from the experimental platform, and the estimated torque $\hat{\boldsymbol{\tau}}(t)$ and estimated position signals $\hat{\boldsymbol{q}}(t)$, $\hat{\boldsymbol{\phi}}(t)$, are used to generate the prediction errors as shown in Fig. 5. The block 'e_{RMS} calculation' indicates the operations required to apply formula (31) using the error signals.

https://doi.org/10.1017/S0263574717000224 Published online by Cambridge University Press

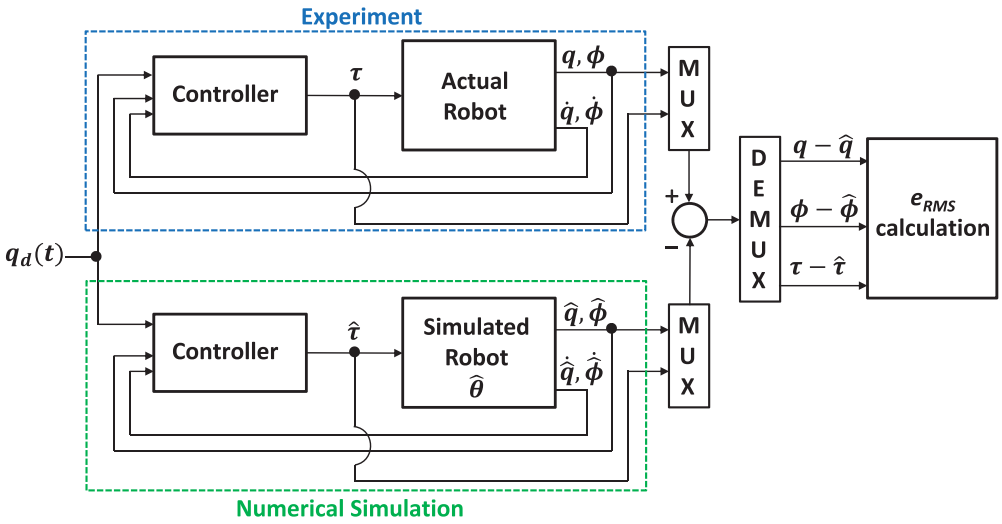

Fig. 5. Block diagram of the validation scheme. The error signals $\boldsymbol{q} - \hat{\boldsymbol{q}}$, $\boldsymbol{\phi} - \hat{\boldsymbol{\phi}}$, $\boldsymbol{\tau} - \hat{\boldsymbol{\tau}}$, generated from the actual and the simulated robot model, are used to compute the corresponding e_{RMS} error values.

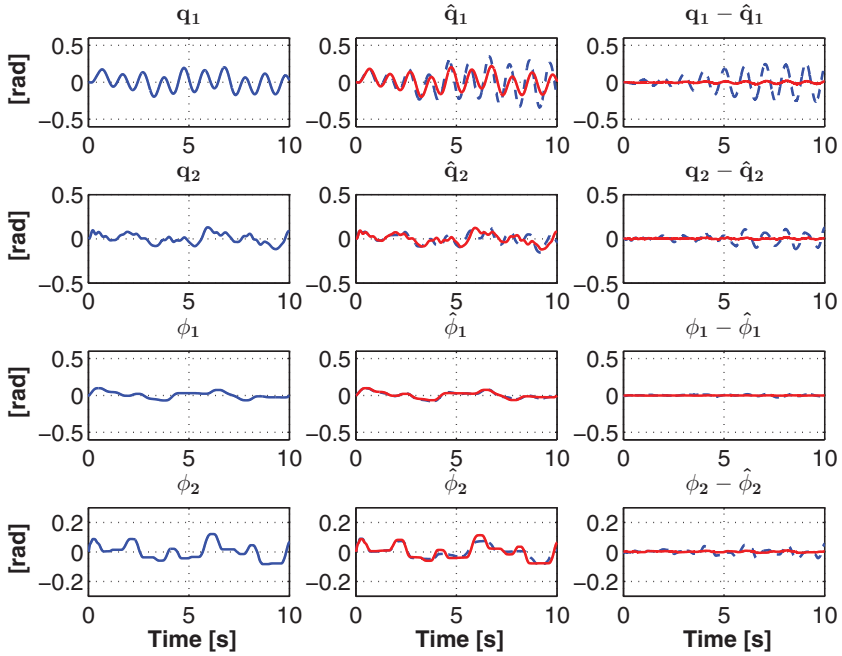

Fig. 6. Direct validation: Measured and estimated values of the link position $\boldsymbol{q}(t)$ and the rotor position $\boldsymbol{\phi}(t)$ by using the proposed identification method (red line) and the LSFF identification scheme (dashed blue line). The error between the actual and simulated position values is also depicted.

4.1. Direct validation

In order to apply the DV approach, we simulated the mathematical model of the FJR manipulator given in Eq. (1). The parameters used in this simulation correspond to the obtained from the proposed identification procedure (denoted by $\hat{\boldsymbol{\theta}}$), and the parameters given by the LSFF identification method (which we represented by $\hat{\boldsymbol{\theta}}_{LSFF}$). See Table III for the numerical values of the estimated parameters $\hat{\boldsymbol{\theta}}$ and $\hat{\boldsymbol{\theta}}_{LSFF}$. The simulation considered the same conditions as in the parameter identification experiment. Then, we compared the link position, rotor position, and torque values using the numerical data obtained from the simulation and the experimental data. Since in the LSFF identification method $\hat{\theta}_7(t)$ is negative, we have performed the simulation with $\hat{\theta}_6 = 0$ in the FJR model. Otherwise the closed-loop system is unstable. Figure 6 shows the measured and simulated rotor and link position

https://doi.org/10.1017/S0263574717000224 Published online by Cambridge University Press

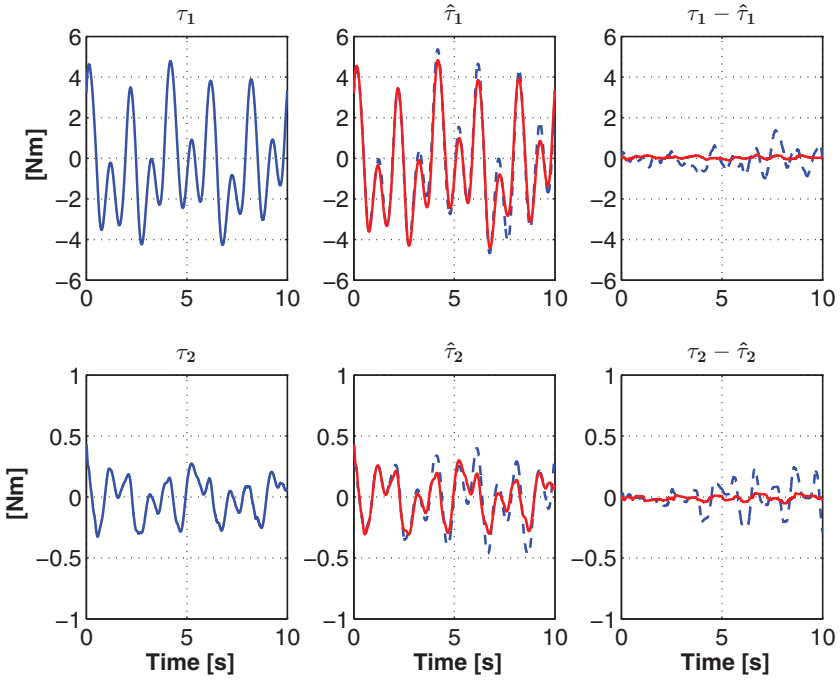

Fig. 7. Direct validation: Measured and estimated torques at the joints by using the proposed identification method (red line) and the LSFF identification scheme (dashed blue line). The error between the actual and simulated torque values is also depicted.

values denoted as $\boldsymbol{\phi}(t), \boldsymbol{q}(t)$ and $\hat{\boldsymbol{\phi}}(t), \hat{\boldsymbol{q}}(t)$, respectively. Figure 7 shows measured torque and simulated torque, expressed by $\boldsymbol{\tau}(t)$ and $\hat{\boldsymbol{\tau}}(t)$, respectively. The error between measured and estimated rotor positions, link positions and torques is also included in both Figs. 6 and 7.

We observe in Figs. 6 and 7 that small error values are obtained for the proposed identification method, indicating that the set of estimated parameters allows constructing a model more suitable for model-based control and dynamic task optimization. However, in order to verify the generalization of the estimated model, the torque and position prediction accuracy approach is also used.

4.2. Torque and position prediction accuracy

Now, the estimated parameters obtained with the proposed approach and the LSFF identification scheme are validated by using a different reference signal and tracking controller. Towards this end, we selected the motion controller presented in ref. [32]. This is a model-based tracking controller based on feedforward compensation plus linear feedback of the state error. The controller design follows the same lines given in ref. [32] and uses the model (1) without the friction terms. The goal is to achieve asymptotic link trajectory tracking, where $\boldsymbol{q}_d(t) \in \mathbb{R}^2$ denotes the desired link trajectory. The nominal rotor trajectory, and its first and second time derivatives are given by

$$\begin{aligned}
\boldsymbol{\phi}_d &= \boldsymbol{q}_d + K^{-1}\boldsymbol{w}_d, \\
\dot{\boldsymbol{\phi}}_d &= \dot{\boldsymbol{q}}_d + K^{-1}\dot{\boldsymbol{w}}_d, \\
\ddot{\boldsymbol{\phi}}_d &= \ddot{\boldsymbol{q}}_d + K^{-1}\ddot{\boldsymbol{w}}_d,
\end{aligned}$$

where $\boldsymbol{\phi}_d \in \mathbb{R}^2$ is the desired rotor trajectory, with

$$\boldsymbol{w}_d(t) = M_1(\boldsymbol{q}_d)\ddot{\boldsymbol{q}}_d + C_A(\boldsymbol{q}_d, \dot{\boldsymbol{q}}_d)\dot{\boldsymbol{q}}_d + \boldsymbol{g}(\boldsymbol{q}_d).$$

https://doi.org/10.1017/S0263574717000224 Published online by Cambridge University Press

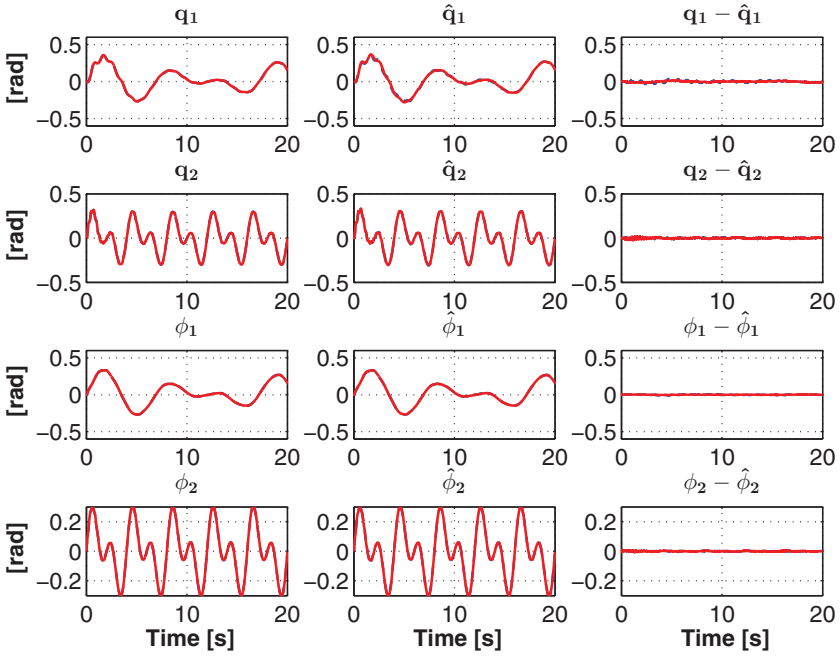

Fig. 8. Torque and position prediction accuracy: Measured link position $\boldsymbol{q}(t)$, measured rotor position $\boldsymbol{\phi}(t)$, predicted link position $\hat{\boldsymbol{q}}(t)$, predicted rotor position $\hat{\boldsymbol{\phi}}(t)$, link estimation error $\boldsymbol{q}(t) - \hat{\boldsymbol{q}}(t)$, and rotor estimation error $\boldsymbol{\phi}(t) - \hat{\boldsymbol{\phi}}(t)$ for the proposed identification method (red line) and the LSFF identification scheme (dashed blue line).

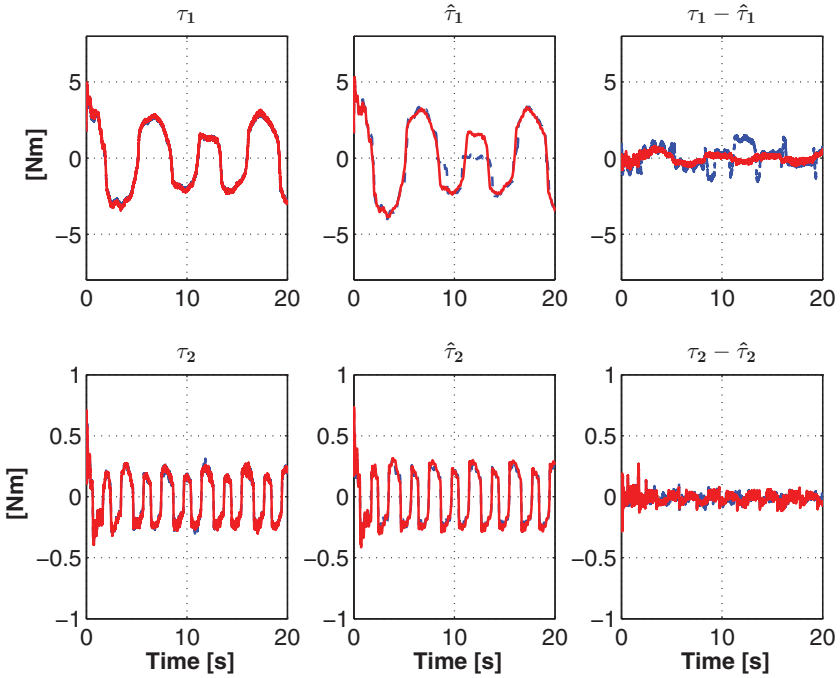

Fig. 9. Torque and position prediction accuracy: Measured torque $\boldsymbol{\tau}$, predicted torque $\hat{\boldsymbol{\tau}}$, and torque prediction error $\boldsymbol{\tau} - \hat{\boldsymbol{\tau}}$ for the proposed identification method (red line) and the LSFF identification scheme (dashed blue line).

https://doi.org/10.1017/S0263574717000224 Published online by Cambridge University Press

Table IV. RMS values of the direct validation method (DV) and the torque and position prediction error (TPPE), using the estimated parameters obtained from the proposed method and the LSFF identification scheme.

		τ_1	τ_2	q_1	q_2	ϕ_1	ϕ_2
DV	e_{RMS} (Proposed)	0.069	0.020	0.010	0.005	0.001	0.004
	e_{RMS} (LSFF)	0.456	0.106	0.130	0.050	0.009	0.021
TPPE	e_{RMS} (Proposed)	0.274	0.036	0.006	0.005	0.001	0.002
	e_{RMS} (LSFF)	0.690	0.036	0.011	0.006	0.003	0.002

The nominal torque for the given trajectory $\boldsymbol{q}_d(t)$ is computed in closed form using the second set of equations in Eq. (1), i.e.,

$$\boldsymbol{\tau}_d(t) = M_2\ddot{\boldsymbol{\phi}}_d + K(\boldsymbol{\phi}_d - \boldsymbol{q}_d), \tag{32}$$

where the friction terms have been neglected.

Therefore, the control law is

$$\boldsymbol{\tau} = \boldsymbol{\tau}_d + F \begin{bmatrix} \boldsymbol{q}_d - \boldsymbol{q} \\ \boldsymbol{\phi}_d - \boldsymbol{\phi} \\ \dot{\boldsymbol{q}}_d - \dot{\boldsymbol{q}} \\ \dot{\boldsymbol{\phi}}_d - \dot{\boldsymbol{\phi}} \end{bmatrix}, \tag{33}$$

where $F \in \mathbb{R}^{2\times 8}$ is a stabilizing gain matrix. Experiments were performed using the desired link signal

$$\boldsymbol{q}_d(t) = 10 \begin{bmatrix} \sin(\frac{\pi}{3}t) + \sin(\frac{\pi}{4}t) \\ \sin(\pi t) + \sin(\frac{\pi}{2}t) \end{bmatrix} [deg],$$

and the stabilizing matrix

$$F = \begin{bmatrix} 50 & 0 & 300 & 0 & 5 & 0 & 0.1 & 0 \\ 0 & 15 & 0 & 40 & 0 & 0.1 & 0 & 0.1 \end{bmatrix}.$$

Figure 8 shows the measured position, predicted position, and the corresponding position prediction errors when using the controller Eq. (33), which were computed by using the estimated parameters obtained with the proposed identification method and the LSFF identification scheme. Let us notice that for the results using the estimated parameters provided by the novel procedure, a good link trajectory tracking accuracy is obtained, and only small vibrations due to flexibility are exhibited. Besides, Fig 9 depicts the measured and predicted actuator torque, and the corresponding torque prediction errors. Finally, Table IV shows the RMS values of the actuator torque prediction error and position prediction error for the DV method, and the torque and position prediction accuracy approach. There, smaller numerical values for all metrics are given for the proposed identification scheme.

Validation has shown that the model obtained with the proposed method allows predicting the actuator torque and position. Therefore, the identified model is well suited for model-based control and dynamic task optimization.[21]

In practice, it is clear that robot manipulators are affected by different types of disturbances and noise that may compromise the identification process. Reasons for the robustness of the proposed identification methodology are explained as follows. In order to lessen the negative effect of the encoder noise present in the position measurements, the rotor and link velocities are estimated on-line and off-line in the experiment for data collecting and in the identification test, respectively, as indicated in Section 2. On the other hand, the negative effect of the PWM switching of the servo amplifier, which introduces noise to the control action, was diminished in the use of the filtered regression model (23) through the filter $f_D(z)$ in Eq. (19), which is a low

https://doi.org/10.1017/S0263574717000224 Published online by Cambridge University Press

pass filter. In summary, the data preprocessing stage developed for the proposed identification methodology allows obtaining a set of reliable estimated parameters, even in the presence of disturbances.

5. Conclusion

We have presented a systematic procedure to effectively estimate the dynamic parameters of a n-DOF FJR manipulator. With the aim of complementing the existing works for parameter identification of FJR manipulators, this paper has covered and explained concisely all the steps required to apply the parameter identification process. The estimated parameters obtained by using the proposed methodology have been shown to be reliable and accurate, which was done by a numerical and experimental study of validation. Besides, the proposed parameter identification scheme was compared with respect to a LSFF identification algorithm.

The proposed parameter identification methodology used a filtered model that does not require acceleration measurements. In the motion control experiments, link and rotor velocity were computed on-line by using an averaging estimator. On the other hand, in the proposed off-line identification procedure, link and rotor velocity were computed with the central differentiation algorithm.

The validation experiments showed that, despite the disturbances, the proposed methodology yields reliable parameter estimates.

In ref. [49], the identification procedure discussed in this paper has been successfully adapted to be used in the estimation of the model parameters of some underactuated mechanisms, such as the Furuta pendulum and the inertia wheel pendulum.

Acknowledgements

This work was supported by CONACyT Project Cátedras 1537 and CONACyT Project 176587.

References

1. G. A. Pratt and M. M. Williamson, "Series Elastic Actuators," *Intelligent Robots and Systems 95. 'Human Robot Interaction and Cooperative Robots', Proceedings. IEEE/RSJ International Conference*, Pittsburg, USA (Aug. 5–9, 1995) pp. 399–406, doi: 10.1109/IROS.1995.525827.
2. A. Albu-Schäffer and G. Hirzinger, "Parameter Identification and Passivity Based Joint Control for a 7DOF Torque Controlled Light Weight Robot," *Proceedings of the IEEE International Conference on Robotics & Automation*, Seoul, Korea (May 21–26, 2001) pp. 2852–2858, doi: 10.1109/ROBOT.2001.933054.
3. B. Siciliano, L. Sciavicco, L. Villani and G. Oriolo, *Robotics: Modeling, Planing and Control*, 3rd ed. (Springer, London, 2008) doi: 10.1007/978-1-84628-642-1.
4. A. Albu-Schäffer and G. Hirzinger, "State Feedback Controller for Flexible Joint Robots: A Globally Stable Approach Implemented on DLR's Light-Weight Robots," *Proceedings of the 2000 IEEE/RSJ International Conference on Intelligent Robots and Systems*, Takamatsu, Japan (Nov. 2000) pp. 1087–1093, doi: 10.1109/IROS.2000.893164.
5. B. Brogliato, R. Ortega and R. Lozano, "Global tracking controllers for flexible-joint manipulators: A comparative study," *Automatica* **31**(7), 941–956 (1995), doi: 10.1016/0005-1098(94)00172-F.
6. Z. H. Jiang and K. Shinohara, "Workspace Trajectory Tracking Control of Flexible Joint Robots Based on Backstepping Method," *Proceedings of the IEEE Region 10 Conference (TENCON)*, Singapore (2016) pp. 3473–3476, doi: 10.1109/TENCON.2016.7848700.
7. A. H. Korayem, M. I. Rahagi, H. Babaee and M. H. Korayem, "Maximum load of flexible joint manipulators using nonlinear controllers," *Robotica* **35**(1), 119–142 (2017) doi: 10.1017/S0263574715000028.
8. C. Ott, A. Albu-Schäffer, A. Kugi and G. Hirzinger, "On the passivity-based impedance control of flexible joint robots," *IEEE Trans. Robot.* **24**(2), 416–429 (2008) doi: 10.1109/TRO.2008.915438.
9. A. Albu-Schäffer, C. Ott and G. Hirzinger, "A unified passivity-based control framework for position, torque and impedance control of flexible joint robots," *Int. J. Robot. Res.* **26**(1), 23–39 (2007) doi: 10.1177/0278364907073776.
10. S. Y. Lim, D. M. Dawson, J. Hu and M. S. de Queiroz, "An adaptive link position tracking controller for rigid-link flexible-joint robots without velocity measurements," *IEEE Trans. Syst. Man Cybern.-Part B: Cybern.* **27**(3), 412–427 (1997) doi: 10.1109/3477.584949.
11. A. C. Huang and Y. C. Chen, "Adaptive sliding control for single-link flexible-joint robot with mismatched uncertainties," *IEEE Trans. Control Syst. Technol.* **12**(5), pp. 770–775 (2004) doi: 10.1109/TCST.2004.826968.

12. R. Lozano and B. Brogliato, "Adaptive control of robot manipulators with flexible joints," *IEEE Trans. Autom. Control* **37**(2), 174–181 (1992) doi: 10.1109/9.121619.
13. K. Khorasani, "Adaptive control of flexible-joint robots," *IEEE Trans. Robot. Autom.* **8**(2), 250–267 (1992) doi: 10.1109/70.134278.
14. H. Liu, Y. Huang and W. Wu, "Improved Adaptive Output Feedback Controller for Flexible-Joint Robot Manipulators," *Proceedings of the IEEE International Conference on Information and Automation (ICIA)*, Ningbo, China (Aug. 1–3, 2016) pp. 1653–1658, doi: 10.1109/ICInfA.2016.7832083.
15. Raouf, F., Mohamad, S., Maarouf, S. and Maamar, B. "Distributed adaptive control strategy for flexible link manipulators," *Robotica* 1–23 (2016) doi: 10.1017/S0263574716000448.
16. L. Zouari, H. Abid and M. Abid, "Sliding mode and PI controllers for uncertain flexible joint manipulator," *Int. J. Autom. Comput.* **12**(2), 117–124 (2015) doi: 10.1007/s11633-015-0878-x.
17. I. H. Akyüz, Z. **B**ingül and S. **K**i**z**i**r**, "Cascade fuzzy logic control of a sinlge-link-flexible-joint manipulator," *Turk. J. Electr. Eng. Comput. Sci.* **20**(5), (2012) doi: 10.3906/elk-1101-1056.
18. J. T. Agee, Z. **B**ingül and S. **K**i**z**i**r**, "Higher-order differential feedback control of a flexible-joint manipulator," *J. Viber. Control* **21**(10), 1976–1986 (2013) doi: 10.1177/1077546313504979.
19. M. B. Leahy and G. N. Saridis, "Compensation of industrial manipulator dynamics," *Int. J. Robot. Res.* **8**, 73–84 (1989) doi: 10.1177/027836499000900406.
20. F. Caccavale and P. Chiacchio, "Identification of dynamic parameters and feedforward control for a conventional industrial manipulator," *Control Eng. Pract*. **2**(6), 1039–1050 (1994) doi: 10.1016/0967-0661(94)91626-8.
21. J. Swevers, W. Verdonck and J. D. Schutter, "Dynamic model identification for industrial robots," *IEEE Control Syst. Mag*. **27**(5), 58–71 (2007) doi: 10.1109/MCS.2007.904659.
22. Z. Bingül and O. Karahan, "Dynamic identification of Staubli RX-60 robot using PSO and LS methods," *Expert Syst. Appl.* **38**, 4136–4149 (2011) doi: 10.1016/j.eswa.2010.09.076.
23. J. Wu, J. Wang and Z. You, "An overview of dynamic parameter identification of robots," *Robot. Comput.-Integr. Manuf*. **26**, 414–419 (2010) doi: 10.1016/j.rcim.2010.03.013.
24. J. Swevers, C. Ganseman, D. B. Tukel, J. D. Schutter and H. V. Brussel, "Optimal robot excitation and identification," *IEEE Trans. Robot. Autom.* **13**(5), 730–740 (1997) doi: 10.1109/70.631234.
25. M. T. Pham, M. Gautier and P. Poignet, "Identification of Joint Stiffness with Band Pass Filtering," *Proceedings of the 2001 IEEE International Conference on Robotics & Automation*, Seoul Korea (May 21–26, 2001) doi: 10.1109/ROBOT.2001.933056.
26. C. Lightcap and S. Banks, "Dynamic Identification of a Mitsubishi PA10-6CE Robot using Motion Capture," *Proceedings of the 2007 IEEE/RSJ International Conference on Intelligent Robots and Systems*, San Diego, CA, USA (Oct. 29–Nov. 2, 2007) doi:10.1109/IROS.2007.4399425.
27. M. Ruderman, F. Hoffmann and T. Bertram, "Modeling and identification of elastic robot joints with hysteresis and backlash," *IEEE Trans. Indust. Electron.* **56**(10), (2009) doi: 10.1109/TIE.2009.2015752.
28. P. van Zutven, D. Kostić and H. Nijmeijer, "Parameter Identification of Robotic Systems with Series Elastic Actuators," *Proceedings of the 8th IFAC Symposium on Nonlinear Control Systems*, Bologna, Italy (2010) pp. 350–355, doi: 10.3182/20100901-3-IT-2016.00127.
29. C. Gaz, F. Flacco and A. De Luca, "Identifying the Dynamic Model used by the KUKA LWR: A Reverse Engineering Approach," *Proceedings of the IEEE International Conference on Robotics and Automation*, Hong Kong (May 31–Jun. 7, 2014) pp. 1386–1392, doi: 10.1109/ICRA.2014.6907033.
30. L. Zollo, E. Lopez, L. Spedaliere, N. G. Aracil and E. Guglielmelli, "Identification of dynamic parameters for robots with elastic joints," *Adv. Mech. Eng.* **7**(2), (2015) doi: 10.1155/2014/843186.
31. `http://www.quanser.com/products/2dof_serial_flexible_joint.`
32. C. Canudas, B. Siciliano and G. Bastin, *Theory of Robot Control* (Springer Verlag, London, 1996) doi: 10.1007/978-1-4471-1501-4.
33. M. W. Spong, "Modeling and control of elastic joint robots," *J. Dyn. Sys. Meas. Control* **109**(4), pp. 310–318 (1987) doi: 10.1115/1.3143860.
34. J. J. Craig, *Introduction to Robotics: Mechanics and Control*, 3rd ed. (Prentice Hall, 2004) ISBN: 978-0201543612.
35. R. Miranda, *Cinemática y Dinámica de Robots Manipuladores* (Alfaomega, 2016) ISBN: 978-607-622-048-1.
36. R. Kelly, V. Santibañez and A. Loría, *Control of Robot Manipulators in Joint Space* (Springer Verlag, London, 2005) doi: 10.1007/b135572.
37. L. Sciavicco and B. Siciliano, *Modeling and Control of Robot Manipulators*, 2nd ed. (McGraw-Hill, London: Springer-Verlag, 2000) doi: 10.1007/978-1-4471-0449-0.
38. J. Moreno-Valenzuela and R. Campa, "Two classes of velocity regulators for input-saturated motor drives," *IEEE Trans. Indust. Electron*. **56**(6), (2009) doi: 10.1109/TIE.2009.2016515.
39. W. Khalil and E. Dombre, *Modeling, identification and Control of Robots*, 3rd ed. (Taylor & Francis, Bristol, 2002) ISBN: 978-1-903996-66-9.
40. C. G. Atkeson, C. H. An and J. M. Hollerbach, "Estimation of inertial parameters of manipulator loads and links," *Int. J. Robot. Res.* **5**(3), pp. 101–119 (1986) doi: 10.1177/027836498600500306.
41. A. De Luca and W. Book, "Robots with Flexible Elements," **In**: *Springer Handbook of Robotics* (B. Siciliano and O. Khatib, eds.) (Springer, 2008) pp. 287–319, doi: 10.1007/978-3-540-30301-5.
42. F. Reyes and R. Kelly, "Experimental evaluation of identification schemes on a direct drive robot," *Robotica*. **15**(5), 563–571 (1997) doi: 10.1017/S0263574797000659.

43. S. Chan and H. Chen, "An Efficient Algorithm for Identification of SCARA Robot Parameters Including Drive Characteristics," *Proceedings of the 25th Annual Conference of the IEEE Industrial Electronics Society*, San Jose, CA, USA (1999) pp. 1014–1019, doi: 10.1023/A:1013918927148.
44. G. L. Iagnemma, S. Dubowsky and G. Morel, "A Base Force/Torque Sensor Approach to Robot Manipulators Inertial Parameter Estimation," *Proceedings of the IEEE International Conference on Robotics and Automation*, Leuven, Belgium (May 16–20, 1998) pp. 3316–3321, doi: 10.1109/ROBOT.1998.680950.
45. R. C. Dorf and R. H. Bishop, *Modern Control Systems* (Addison Wesley, Menlo Park, California, 1998) ISBN: 978-0136024583.
46. M. Gautier, A. Janot and P. O. Vandanjon, "A new closed loop output error method for parameter identification of robot dynamics," *IEEE Trans. Control Syst. Technol*. **21**, pp. 428–444 (2013) doi: 10.1109/TCST.2012.2185697.
47. E. Ikonen and K. Najim, *Advanced Process, Identification and Control*, Automation and Control Engineering, 1st ed. (CRC Press, 2001) ISBN: 978-0824706487.
48. P. A. Ioannou and J. Sun, "Robust Adaptive Control," **In**: *Dover Books and Electrical Engineering*, 1st ed. (Dover Publications, 2012) ISBN: 978-0486498171.
49. J. Moreno-Valenzuela and C. Aguilar-Avelar, *Motion Control of Underactuated Mechanical Systems* (Springer Science Business Media, in press to be published, 2017).